 CMES, vol.50, no.1, pp.67-96, 2009

Modeling of the Inhibition-Mechanism Triggered by 'Smartly' Sensed Interfacial Stress Corrosion and Cracking

Sudib K. Mishra[1], **J. K. Paik**[2] **and S. N. Atluri**[1]

Abstract: We present a simulation based study, by combining several models involving multiple time scales and physical processes, which govern the interfacial stress corrosion cracking (SCC) in grain boundaries, layered composites or bi-materials, and the mechanisms of inhibition using 'smart' agents. The inhibiting agents described herein, automatically sense the initiation of damage, migrate to the sites and delay the corrosion kinetics involved in the process. The phenomenon of SCC is simulated using the lattice spring model (for the mechanical stresses), coupled with a finite difference model of diffusing species, causing the dissolution of the interfacial bonds. The dissolution is expressed through a kinetic rate equation, which is solved stochastically using the kinetic Monte Carlo (kMC) to explore the fine selectivity of the evolution. Two alternative sensing mechanisms are employed, along the lines of the previous investigators; (a) the interactions among the inhibitor and the species and (b) the interaction of the inhibitors with the catalyst released under the action of the enhanced stress around the propagating crack front. Alternative forms of an empirically defined potential are used to model the chemical potential differences responsible for the driving force of migration. The inhibitor which migrates to the crack front initiates counter-dissolution kinetics (dealt with the kMC) to enforce the inhibition. The inhibition is quantified in terms of the time demand of these two competing kinetics (dissolution-inhibition). The robustness of the migration-inhibition is qualitatively inferred with respect to the random allocations of inhibitors in the domain.

Keywords: Interfaces, Stress Corrosion, Crack, Monte Carlo, Lattice Spring Model, Boltzmann Equation, Corrosion Inhibition

[1] Center for Aerospace Research & Education, University of California, Irvine
[2] Lloyd's Register Educational Trust (LRET) Research Center of Excellence, Pusan National University

1 General

The concepts of autonomous corrosion-inhibition [Jakab and Scully (2005), Zheludkevich, Serra, Mon-temayor, Yasakau, Miranda-Salvado and Ferreira (2005), Lamaka, Shchukin, Andreeva, Zheludkevich, Mohwald and Ferreira (2008), Brown, White and Sottos (2005), Dry (1994), White, Sottos, Geubelle, Moore, Kessler, Sriram, Brown and Viswanatham(2001), Gutpa, Zhang, Emrick, Balazs and Russell (2006), Lee, Buxton and Balazs (2004)] are currently being considered for the prevention of corrosion induced damage of engineering materials such as composites, metals and refractory materials (e.g silica). These new technologies have the potential to replace the traditional inhibition systems, which were primarily based on coating, painting or electroplating Technologies [Fontana (1986)]. Compared to their primitive counterparts, these new inhibition options could fulfill the stringent environmental regulations, and function based on automatic damage sensing principles [Dry (1994)]. They alleviate the need for periodic inspections, and can be used economically through a feedback loop mechanism based on smart sensing. Most of these inhibitors work on the 'release on demand' [Jakab and Scully (2005)] principle, and may be grouped under 'smart' inhibition strategy [White, Sottos, Geubelle, Moore, Kessler, Sriram, Brown and Viswanatham (2001)].

However, most of these technologies are still in their infancy, and an exploitation of such mechanisms requires extensive interdisciplinary research to explore the complex underlying scientific principles, robustness of the performance and efficiency. The key engineering challenge is to understand and extract the fundamental functional aspects of the systems in order to develop an inhibition strategy that can feasibly and cost-effectively be applied to engineering structures. The Multiphysics nature of the problem arises out of the different processes involved in the problem [Trenado, Strauss and Wittmar (2008), Nishidate and Nikishkov (2008)] and the Multiscale nature is due to the characteristic time scales associated with the ambient physics [Trenado, Strauss and Wittmar (2008), Srivastava and Atluri (2002), Fitzgerald et al.(2008)]. Given these facts, the simulation of such a problem must be performed in a Multiscale, Multiphysics framework which forms the object of the present study.

We consider the problem of SCC under the combined actions of the ingressing chemical species through diffusion, and the mechanical stresses at the interfaces commonly encountered in composites, grain boundaries in a microstructure and in layered or bi-materials [Kamaya, Itakura (2009)]. The ingress of chemicals is through the diffusion mass transfer along the interface. The chemical bonding between the materials deteriorates under the dissolution/accretion by the diffusing chemical [Yakobson and Shchukin (1993)]. The rate of dissolution is highly influenced by the stresses. Higher stress levels increase the rate of dissolution, to

accelerate the processes, thus facilitating the propagation of the crack. This is the main characteristic of the phenomenon of the stress assisted corrosion cracking [Kamaya, Itakura (2009)]. Dissolved bonds make room for further diffusion, resulting in an ever increasing stress accompanied by dissolution rates leading to catastrophic failure through sudden appearance of brittle macroscopic cracks.

The inhibition strategy presently studied in this paper is based on the smart sensing strategy of the inhibiting agents (e.g nanoparticles [Gutpa, Zhang, Emrick, Balazs and Russell (2006)], microcapsules [Brown, White and Sottos (2005)], catalytic agents, polyelectrolyte [Lamaka, Shchukin, Andreeva, Zheludkevich, Mohwald, and Ferreira (2008)]. These inhibitors are triggered to move to the location of the SSC under the action of some kind of driving force (derived from the chemical potential difference, diffusion, concentration gradient, potential gradient and so on). The way in which such driving forces are engineered for a smart sensing strategy varies widely. Nonetheless, once these inhibitors reach to the sites of the SCC front, they take part in the kinetics at the progressing crack tip, to retard the kinetics. Such a retardation or complete stoppage of the kinetics ultimately results in the arrest of the propagating SCC front at the interface. This is the basic phenomenon of SCC and the Inhibition mechanism currently being studied. The study uses a combined simulation framework of several numerical schemes (Lattice spring model for the cracking, finite difference for the corrodent diffusion, Lattice Boltzmann Model (LBM) for the Inhibitor migration, and kinetic Monte Carlo for the corrosion and inhibition kinetics) to capture the different physics mutually interacting at their characteristic scales. The phenomenon of SCC, sensing of the SCC damage, migration of Inhibitors to the crack front and the competing nature of the dissolution-inhibition kinetics, are simulated, and it is shown how in combination, they ultimately lead to the arrest of the corrosion crack front. The basic models and methods are presented, along with their interrelation and exchange of information through the hand shake region. The results are presented along with discussions to indicate the efficacy of the proposed simulation, and the inhibition strategy.

2 Models and Methods

With the multiscale, multiphysics flavor of the problem having been emphasized, we provide an algorithmic Flow Chart for the coupled framework in Figure 1 where the models/methods, the migration of informations along mutually interacting scale/physics is schematically depicted.

As indicated in this flow chart, the simulation starts with the assumption of an initial concentration of the corroding chemical species and the previously distributed inhibitors inside the domain. The algorithm for the dissolution kinetics is initiated to estimate the time demand of the dissolution. The time demand is compared with

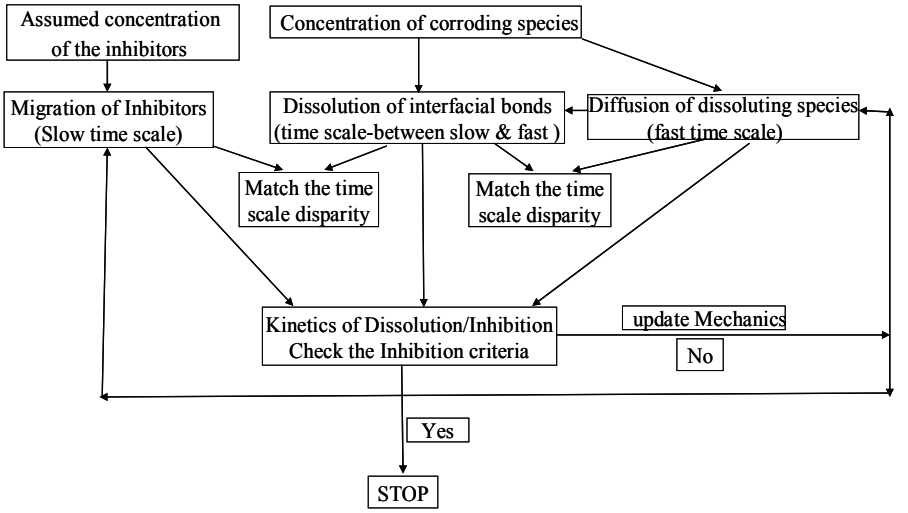

Figure 1: The Flow Chart of the Multiscale and Multiphysics Modeling Framework

the permissible time step of the diffusion simulation as well as the time steps for inhibitor migration, the analysis of which is based on the LBM. The disparities in the time scales, are bridged by the 'brute force bridging', meaning the slower ones are allowed to run until the faster ones are matched. The faster ones are A_s thus sandwiched between the slower time scales. Once the scales are bridged among all three processes, the system is updated and the time demand for the Inhibition mechanism is evaluated at the propagating crack front. This is checked with the simultaneously active dissolution time demand to conclude on the degree of Inhibition. If the criterion of Inhibition is satisfied, the simulation comes to an end, otherwise the system is updated with the dissoluted bonds (crack propagates), to evaluate the modified state of stress. With this new state of stress, species concentrations, and the state of inhibitor migration, the same steps are repeated until the criterion of Inhibition is enforced. These constitute the basic simulation of corrosion Inhibition described herein. Individual descriptions of the models and methods are detailed subsequently.

2.1 Ingress of the corroding species through interfacial diffusion

The diffusion of the chemical species responsible for the dissolution of the interfacial bonds is described through the diffusion equation, solved on a two dimensional finite difference grid discretizing the domain. The domain with the material interface is shown in Figure 2. The diffusion is considered to be restricted along

the interface and the size of the domain changes with time, as progressively more bonds get dissolved, making room for more species to diffuse. The basic equation of diffusion in a two dimensional domain is given by

$$\frac{\partial C}{\partial t} = D\left(\frac{\partial^2 C}{\partial x^2} + \frac{\partial^2 C}{\partial y^2}\right) \tag{1}$$

where, $C(x,y)$ is the concentration of the species and D is the diffusion coefficient. Previous studies reveal that species are accommodated at interstitial spaces along the interface and therefore the diffusivity is related to the chemical characteristics of the interstitial spaces. They can be parameterized by more detailed atomistic calculations or from experimental measurements. This can also be a function of the physio-chemical properties of the interfaces and the ambient stresses. The equation is solved numerically in the domain using a Finite Difference (FD) grid discretizing the domain of interest, shown in Figure 2.

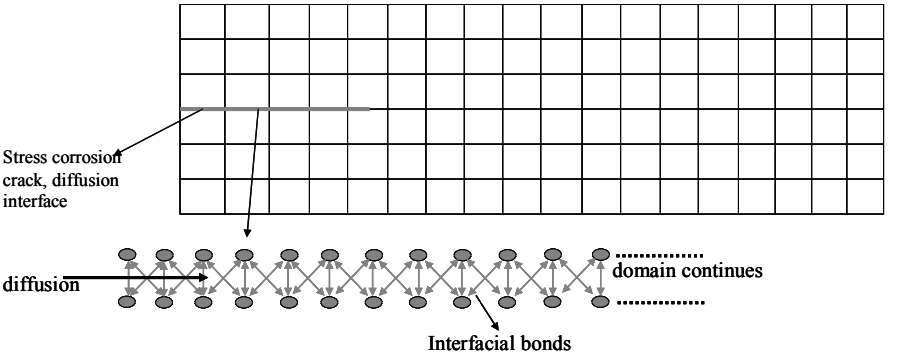

Figure 2: The geometry and lattice discretization of the domain for interfacial diffusion, stress assisted dissolution/cracking and the migration of the Inhibitors

Ingress of chemical species dissolves the interface bonding under local stress conditions leading to an initiation of the crack or growth of the existing ones [Lufrano, and Sofronis (2000)]. As the diffusion progresses and more bond-dissolution occur, the domain widens and the boundary conditions are updated accordingly. This is schematically illustrated in Figure 2. It is intuitive that there might be disparity in time scales associated with the diffusion and stress assisted dissolution. The time steps in the simulation are governed by the diffusion, whereas the lattice configurations, boundary conditions are updated in accordance to the dissolution kinetics.

2.2 The kinetics of interfacial dissolution

Interfaces in the material provide additional degrees of freedom (the atomic mobility along the surface and/or with the environment) and increases the compliance to external effects. The interfacial mass transfer acts in conjunction with the inhomogeneous stresses to change the original configurations of solid body/surfaces and play a determining role in the material-durability. The dissolution of the solid phase is governed by the chemical potential gap between the solute and solid, affected by the stress field. The stresses add local deformation energy to the chemical potential. In addition, concavity on the surface also serves as a stress concentrator to enhance chemical potential. In unison, these factors cause locally enhanced dissolution, growth of the crack and further change of local stress/chemical potential. This feedback (stress field-dissolution-stress) loop leads to the instability of the interface to propagation the self-fracture front.

The change in the chemical potential with respect to the equilibrium configuration is expressed as [Yakobson and Shchukin, (1993)]

$$\Delta\mu = a^3 \left\{ \frac{1}{2E}\left[\sigma^2 - \sigma_0^2\right] - \frac{\gamma}{\rho} \right\} \tag{2}$$

where, a^3 is the atomic volume, σ and σ_0 are non-equillibrium and equilibrium states of stress normal to the interfacial boundary, γ is the surface energy and ρ is the radius of curvature. For the present case, the curvature does not change and the second term can be dropped from the expression. The mass transfer is restricted to the direction normal to the interface. When the solute is in equilibrium with the homogeneously stressed surface, the number of atoms leaving the solid phase equals the number of atoms returning from the solute i.e

$$r_0 = r_{\longrightarrow} = r_{\longleftarrow} \tag{3}$$

Far from the equilibrium (excessively stressed body), the dissolution prevails by changing the activation barrier and hence the forward rate $(r_{\longrightarrow})$

$$\frac{r}{r_0} = \frac{r_{\longrightarrow} - r_{\longleftarrow}}{r_0} = \exp\left[\frac{\Delta\mu}{kT}\right] - 1 \tag{4}$$

where, k is the Boltzmann constant, T is the absolute temperature of the system. Upon linearization, (4) is approximated as

$$\frac{r}{r_0} \approx \frac{\Delta\mu}{kT} = \frac{a^3}{2EkT}\left(\sigma^2 - \sigma_0^2\right) \tag{5}$$

$$r = \frac{r_0 a^3}{2EkT}\left(\sigma^2 - \sigma_0^2\right) \tag{6}$$

with this rate, the dissolution of bonds is idealized as a first order kinetics [Mullin, Shumaker and Tyler(1997)]

$$\frac{dC_{db}}{dt} = -rA_sC_sA_bC_b \tag{7}$$

where, A_s is the activity coefficient of the solute, C_s is the concentration of the solute, A_C is the activity coefficients of the interfaces and C_b is the bond density (here, number of bonds per unit length along the crack). This equation can be solved directly in a mean field sense, which might seem simple but lacks fine intricacies inherent to the atomistic nature of the bond dissolution. More realistic simulations could be via stochastic kinetic Monte Carlo technique. From equation (7), it can be shown that the probability density of the event of interfacial dissolution can be written as

$$p\left(C_{ds}\right) = 1 - \exp\left(-rA_bC_bA_sC_s\Delta t\right) \tag{8}$$

on inversion, the time demand of the events can be written as

$$\Delta t = -\left(\frac{1}{rA_bC_bA_sC_S}\right)\ln\left(1-p\right) \tag{9}$$

With given bond density, local concentration of the solute, the rate of the kinetics and randomly assigned probability (by Monte Carlo) of the event, the time demand of dissolution can be estimated by eqn. 9 to update the system. It is seen that the dissolution rate (r), being a function of the ambient stress at the site, couples the kinetics to the mechanics of the problem. Progressive debonding enhances the interfacial stress to accelerate the process in the feedback loop mentioned earlier.

2.3 Evolution of the Mechanical Stresses at the interface

The interface in a material system is computationally modeled using the Finite element technique through discretization of the continua. Presently, we treat the discrete event of the individual bond dissolution in a mesoscopic regime and a discrete model is necessary for the simulation. The lattice spring model (LSM), which is used for the micromechanical simulation of cracks, scaling phenomena, disorders in solids [Alava, Nukala, Zapperi (2006)] offers such flexibility.

Here we briefly describe the lattice spring model (LSM), consisting of a network of harmonic springs connecting each lattice site or node with its nearest neighbors along axial and diagonal directions, shown in Figure 2 and 3. The Hamiltonian associated with a node i is written as

$$H_i = \sum_j \frac{k_{ij}}{2}\left(u_i - u_j\right)^2 \tag{10}$$

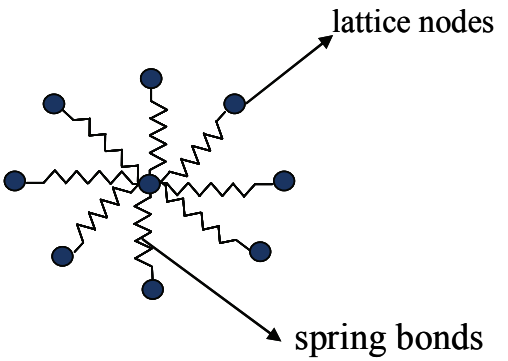

Figure 3: The lattice spring model (LSM) configurations

where, u_i and u_j are the displacements of node i and j from its original/equilibrium positions and k_{ij} is the spring constant of the harmonic spring connecting node i to node j. The summation is carried over all its neighboring nodes (j) for node (i). From a continuum perspective, the system of equations for LSM obeys the linear elasticity and results in a Young's modulus (E) as

$$E = \frac{5k_{ij}^{cen}\left(2k_{ij}^{cen} + 3k_{ij}^{dia}\right)}{\left(4k_{ij}^{cen} + k_{ij}^{dia}\right)} \tag{11}$$

and the Poisson's ratio (ν)

$$\nu = \frac{k_{ij}^{axi} - k_{ij}^{dia}}{k_{ij}^{dia} + 4k_{ij}^{axi}} \tag{12}$$

where k_{ij}^{axi} and k_{ij}^{dia} are the spring constants for the neighbors located along the axial and diagonal directions of node i. With the present lattice configuration (Figure 3), node i has eight neighbors around it, resulting a Poisson's ratio of $\nu = 0.25$, which can be varied by including more complicated many-body interactions.

The lattice nodes are coincident to the finite difference nodes for species diffusion used in the study. The species diffuse along the interfacial boundaries, dissolve the individual bonds (springs), and the system is equilibrated through updating the nodal displacements and stresses in the springs (Figure 2). The time scale of the bond breakage given in equation (9) therefore determines the time-scale of re-equilibration of the lattice system.

2.4 Migration of the Inhibiting Agent

The inhibitors are put in the system a priori to sense the onset and propagation of SCC. Such autonomic sensing triggers a controlled release and migration of the inhibitors to supply counteractive species as a protective agent. The inhibitors are contained as active species in localized reservoir/pockets and released if necessary. Conductive polymers are used as reservoirs for corrosion inhibitors. The release might be triggered by galvanic reduction, ion exchange, changes in pH or interactions induced by the chemical gradients. Such strategy can provide further protection, in addition to the traditional ones. The 'on a demand' release uses a switching mechanism to trigger the inhibitors getting transported to the corroding sites. The switching mechanism could be diffusion under concentration gradients, ionic mobility under corrosion induced potential differences or a special kind of philic-interaction of the corroding species towards the inhibiting agents.

The present study relies on two postulated mechanisms for stress corrosion damage sensing, namely: 1. The chemical potential difference between the corrosion species and the inhibiting agents (nanoparticles) stored in the system, and 2. The potential difference among the inhibitors and the catalytic agents released by breakage of the capsules (stored in the system) under enhanced stresses around the moving crack front. The breakage of the capsules is localized around the propagating front due to the higher level of stresses around. These potential differences trigger the active sensing mechanism and the migration of agents to the propagating front.

The transport/migration can efficiently be weaved with the LSM by solving the transport equations for Inhibitor-migration on the same lattice, shown in Figures 2,3, and taking into account the long range interactions among the inhibiting agents and the corroding species/stored catalysts in the system. The transport can be modeled by the Boltzmann Transport equation describing the statistical distribution of particles $(f(\{x\},\{p\},t))$ in their phase space $(\{x\},\{p\})$, where $\{x\},\{p\}$ are respectively the position and momentum of the particles. The evolution of the phase space description can be expressed using the Boltzmann Transport equation

$$\frac{\partial f}{\partial t}+\frac{\partial f}{\partial x}\frac{p}{m}+\frac{\partial f}{\partial p}F=\left|\frac{\partial f}{\partial t}\right|_{coll} \tag{13}$$

where, $F(x,t)$ is the force field acting on the particles, m is the mass of the particle. The term on the right hand side describes the effect of collisions between the particles.

This equation of transport is solved discretely on the lattice nodes [Succi (2001), Ho, Chang and Lin (2009)] using the Lattice Boltzmann Model (LBM). This method is of particular choice here as compared to a full atomistic simulation as in the

Molecular dynamics (MD), due to the fact that the tractable spatial domain using MD is far below than what is typically required for engineering purposes. Moreover, the individual trajectories typical to MD simulation provide a lot more redundant information compared to its physical abstraction [Nishimura and Miyazaki (2001)]. In that sense, the LBM model is more efficient in being a mesoscopic technique which uses the computational ease of a macroscopic solver, yet retaining the atomistic flavour in it. The LBM can be viewed as a coarse grained MD which retains minimal phase space information by treating the aggregate of particles (probability density, f) instead of the individual positions and momentum($\{x\},\{p\}$) of the atoms. Using Chapman-Enskog Multiscale expansion technique it can be shown that in its continuum limit, the LBM mimics the Boltzmann Transport equation (13). The potential-induced interactions (which in turn provide the driving for for the transport (F) in equation (13)) between the species and agents can efficiently modeled through this model.

On this lattice, the macroscopic density of the Inhibitors is discretised into nine bins along the axial and diagonal directions as the probability distribution functions,f_a shown in Figure 3. Such distribution functions can be viewed as the direction–specific densities of aggregation of particles. The macroscopic density is summed up from these directional densities

$$\rho = \sum_{a=1}^{9} f_a \tag{14}$$

The macroscopic velocity (u) of the inhibitors is the average of the microscopic velocities (e_a) weighted by the directional densities (f_a) i.e

$$u = \frac{1}{\rho} \sum_{a=1}^{9} f_a e_a \tag{15}$$

This allows passing the discrete microscopic velocities of the lattice to the macroscopic continuum.

The next operations are streaming/propagation and collision of the Inhibitor particles through the distribution functions. The Bhatnagar-Gross-Krook (BGK) approximation is used for collision [Succi (2001)]. Streaming and collision is used to attain the relaxation of the interacting particles toward local equilibrium, given by

$$f_a(x+e_a\Delta t, t+\Delta t) = f_a(x,t) - \frac{\left(f_a(x,t) - f_a^{eq}(x,t)\right)}{\tau} \tag{16}$$

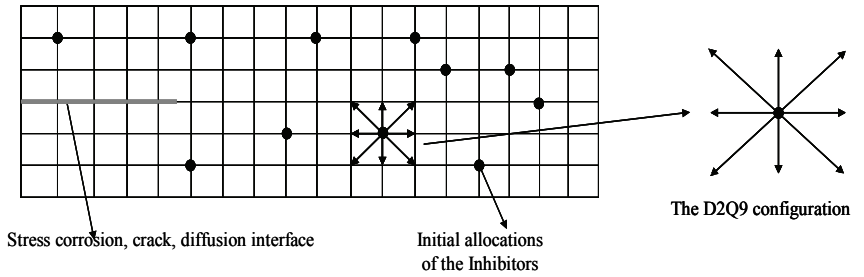

Figure 4: The D2Q9 lattice configurations for the LBM and the velocity components

The right side of equation (16) represents the streaming from one node to its neighbor and the second term is due to collision. Collision can be thought of as relaxation toward local equilibrium and for the D2Q9 (two dimensional, nine directions, shown in Figure 4) lattice the equilibrium distribution function f_a^{eq} is expressed as

$$f_a^{eq}(x) = w_a \rho(x) \left[1 + 3\frac{e_a u}{c^2} + \frac{9}{2}\frac{(e_a u)^2}{c^4} - \frac{3}{2}\frac{u^2}{c^2} \right] \tag{17}$$

where, the weights w_a are $\frac{4}{9}$ for the rest particles$(a = 9)$ at the nodes, $\frac{1}{9}$ for axial directions $a = 1,3,5,7$ and $\frac{1}{36}$ for $a = 2,4,6,8$ for diagonal directions and c is speed of sound on the lattice, taken as 1/3.

The long range interaction (from the difference in chemical potential) between the Inhibitor and the Corrodent is incorporated as an interactive force (F) among nearest neighbor particles as

$$F(x,t) = -G\psi(x,t) \sum_{a=1}^{9} w_a \psi(x + e_a \Delta t, t) \tag{18}$$

where, G denotes the strength of interaction, and ψ is the form of the interaction potential. G<0 leads to attraction and $G > 0$ implies repulsion. The force term in equation (18) is incorporated in the LBM simulation by adding a velocity terms to the existing velocity, following the Newton's equation

$$F(x,t) = \rho(x,t) \frac{d\Delta u_{lr}}{dt} \tag{19}$$

where, $\rho(x,t)$ is the Inhibitor-density on the lattice and Δu_{lr} is the added velocity term due to long range Inhibitors-Species and Inhibitor-Catalyst interactions. Recalling that the relaxation time (τ) is the elementary time of collisions, equation

(19) can be rearranged as

$$\Delta u_{lr}(x,t) = \tau F(x,t)/\rho(x,t) \tag{20}$$

and the total velocity then becomes

$$u_{eq} = u + \Delta u_{lr} \tag{21}$$

This resultant velocity (u_{eq}) is used in computation of the equilibrium probability density function $f_a^{eq}(x,t)$, provided in eqn (17).

Specific forms of the interaction potential causing the transport of the inhibiting species (nanoparticles [Gutpa, Zhang, Emrick, Balazs and Russell (2006), Lee, Buxton and Balazs (2004)], and of the catalysts released from the broken microcapsules [Brown, White and Sottos (2005)]) to the corrosion sites are postulated for quantifying the strength of of the active damage sensing. They can be expressed in any of the following form [Shan, Chen(1993)]

$$\psi(\rho) = \psi_0 \exp(-\rho_0/\rho) \tag{22}$$

$$\psi(\rho) = \rho \tag{23}$$

$$\psi(\rho) = g\rho_0^2\rho^2/\left[2(\rho_0+\rho)^2\right] \tag{24}$$

where, ψ_0 and ρ_0 are constants. With these alternative forms of the potential, the molecular attraction aspect of interactions among the agent and species/catalyst can be included. For the species-inhibitor based interactions, the lattice density of both the species (species s and inhibiting agent a) (ρ_s, ρ_a) have been considered in calculating the interactive forces. For cases, where the inhibition is triggered by the breakage of microcapsules and release of the catalysts [Brown, White and Sottos (2005)], the respective ρ is replaced by the difference of the near field (σ_n) (around the crack front) and the far field stresses (σ_f), multiplied by a parameter (presently taken as constant) quantifying the intensity of the release

$$\rho_a = c(\sigma_n - \sigma_f) \tag{25}$$

where, ρ_a is the density of the catalyst. We note that with this simple expression it is assumed that the release of the inhibiting agent is proportional to the enhanced level of stress around the crack ensuring the rupture of the encapsulated catalysts. Thus, the movement of the inhibitors under the active force field resulting from the damage sensing mechanism of the inhibiting agent can be modeled.

2.5 Condition of Inhibition

The corrosion progresses with the dissolution reaction at the interfaces. The inhibitors migrate to the corrosion site from randomly allocated points inside the domain. These agents take part in counteractive reactions to arrest the corrosion processes [Trenado, Strauss and Wittmar (2008)]. The reaction rates of the counteractive kinetics are known a priori, therefore the simulation of the relevant kinetics can directly follow the kMC, stated in the preceding section to quantify the inhibition kinetics. The counteractive kinetics can be expressed in the following form

$$S + I \xrightarrow{r_{ini}} S - I \tag{26}$$

Where, S is the substrate (here the interfacial bonds) subjected to dissolution, C is the corroding species, I is the inhibiting agent, r and r_{ini} are the rate of the dissolution and inhibition kinetics. The actual reaction mechanism could be quite involved, but they can be merged into apparently simple rate processes. For the SCC, the corrosion reaction is simply the dissolution of bonds detailed in previous section, and the inhibiting agent could act by simply retarding the rate of dissolution or forming a less susceptible precipitate along the interfacial boundaries. The counteractive rate equation can thus be written as

$$\frac{dC_b}{dt} = r_{ini} A_i C_i A_b C_b \tag{27}$$

where, r_{ini} is the rate of the inhibition kinetics, A_i and C_i are the activity coefficient and the local concentration of the inhibitors. Combining the inhibition and the dissolution kinetics, the resulting rate equation can be expressed as

$$\frac{dC_b}{dt} = -rA_s C_s A_b C_b + r_{ini} A_i C_i A_b C_b \tag{28}$$

Following the stochastic formulation, the time demand for the resultant kinetics (competency between the dissolution and inhibition mechanism) is expressed as

$$\Delta t = -\frac{1}{C_b A_b \left(rA_s C_S - r_{ini} A_i C_i\right)} \ln\left(1 - p\right) \tag{29}$$

A description of the degree of inhibition can be obtained from the above expression. From the parameter in the denominator

$$D_i = \left(rA_s C_S - r_{ini} A_i C_i\right) \tag{30}$$

we see that with smaller value of D_i, the time demand of the relevant kinetics in the forward direction (i.e dissolving the interfacial bonds) becomes so large that

the propagation of resulting crack front is abnormally delayed, implying the arrest for all practical purposes. For D_i value less than or equal to zero the time demand becomes undefined, meaning complete cease of the forward kinetics. This is used as a condition for inhibition.

3 Results and Discussion

We demonstrate the coupled multiscale, multiphysics framework in a two dimensional prototype problem of interfacial SCC and its interplay with the inhibition mechanism. The parameters are expressed in arbitrary units of space and time(au). The domain is chosen to represent an interface, with smaller width (6 *au*) and relatively larger length (100 *au*) to simulate the initiation/propagation of the dissolution-assisted instability, cracking and active Inhibition. The LSM for the discrete dissolution of bonds and cracking, the FD method for the interfacial diffusion, and the LBM for the Inhibitor migration are solved on the lattice nodes along with the kMC described kinetics. With the adopted parameters and geometries, the basic phenomena of propagation of cracking, coupled to the species diffusion and the migration of the inhibitors are simulated. Two competing kinetics i.e inhibition and dissolution are localized at the propagating front.

The spatial resolution $(\Delta x, \Delta y)$ of the FD grid is assigned as $0.125au$. The diffusivity of the species responsible for dissolution is taken as $0.005au$. The stiffness of the materials and interface bonds are taken 1500 and 1500 *au* respectively. The parameters adopted for dissolution kinetics are: the atomic volume of the bonds is 20 *au*, the temperature (maintained constant throughout the simulation) is 300 *au* and the dissolution rate is taken as 0.003 *au*. The corroding species are injected initially at one end of the domain with a concentration of $100au$ at the nodes $(y = 3,4, x = 1)$ centrally located along the width at one end of the domain. In general, the allocation of the inhibitors in the domain is random, but, for demonstration purposes we assign the location of the inhibitor reservoir on the lattice nodes with x and y coordinate values ranging from $(y = 2,3, x = 75,85)$. It is assumed that in case, the inhibitor needs triggering by the catalytic action, catalysts are uniformly stored in the domain (in the form of microcapsules) and will only be released under certain level of stress (above the ambient) prevalent around the crack tip. Initial density of $100au$ is assigned for the inhibitors at these nodes. Maintaining the Courant stability criteria, the diffusion time steps for the species causing the dissolution are chosen as $0.01au$ and for the solution of LBM, the lattice time steps are assumed as $2au$.

The ingress of the species along the interface are shown in Figures 5 and 6. The species concentration field is shown in Figure 5, and the time evolution of concentrations at selected points on the interface is shown in Figure 6. The effect of

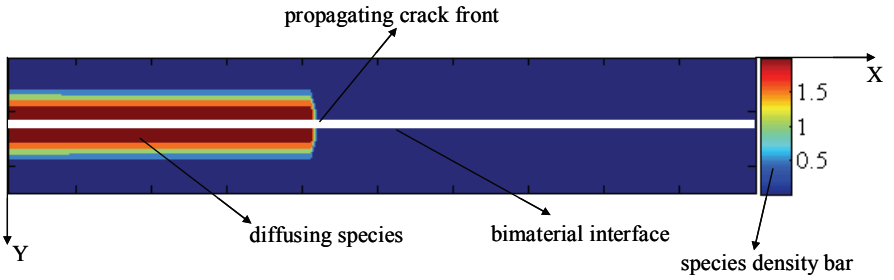

Figure 5: The concentration field of the species ingression along the bimaterial interface (after time 9052) au. The bimaterial interface and the propagating crack front are shown along with the diffusing species. The color bar aside gives the estimate of the species densities

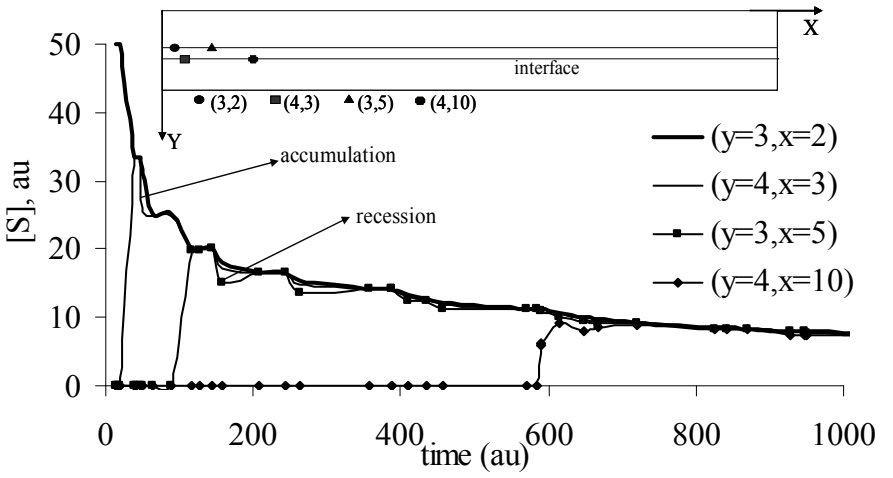

Figure 6: The time evolution of species concentration at selected points along the interface. x and y coordinate of the selected points are indicated and located in a schematic of the domain. The interaction of the diffusion and dissolution time scales is portrayed as the accumulation and recession of the species. With time, concentrations asymptotically reach to the nearly-uniform distributions

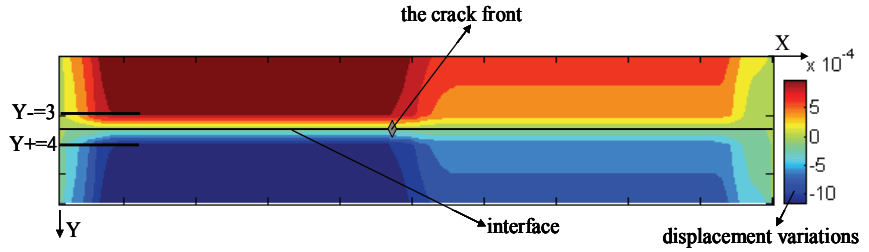

Figure 7: The field variations of the component of the displacement (perpendicular to the crack surface,) around the interface (after t=13263 au). The crack is along the interface marked by the line. The bar aside shows the field variations of displacement in varying color

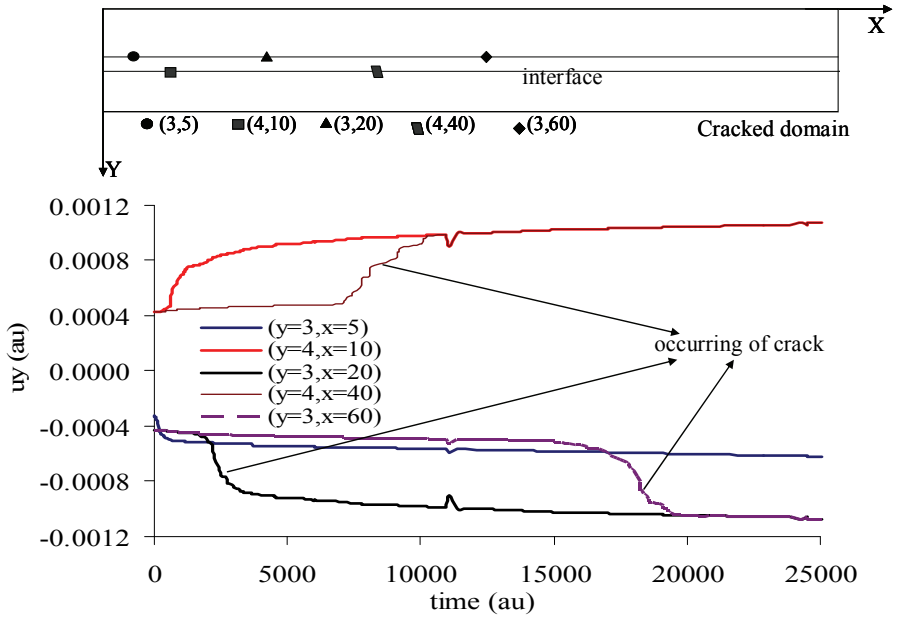

Figure 8: The evolution of the displacement (normal to the crack boundary) at different positions (y,x) in the domain. The points are shown in a schematic of the domain

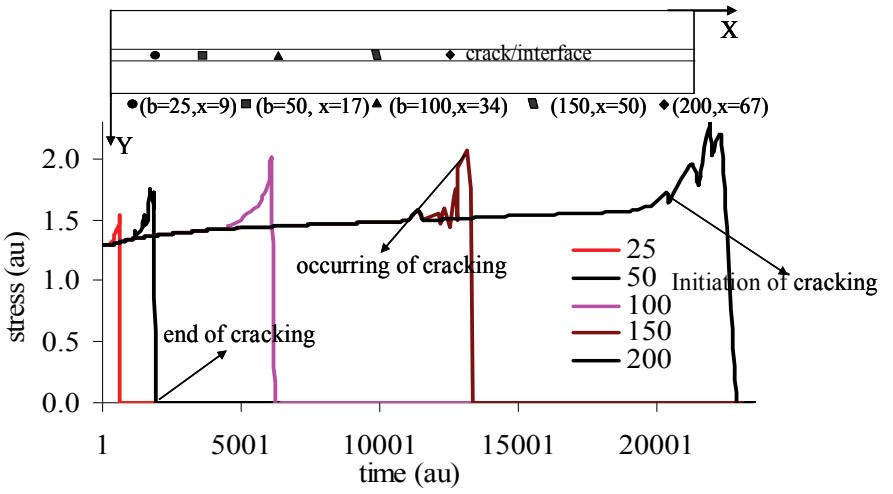

Figure 9: The time evolution of the stresses at the Interfacial elements. The positions of the interfacial elements are mentioned in the figure. The positions of these bonds in the are schematically shown in below [b represents the bonds and x is the x-coordinate (parallel to the crack) corresponding the bond]

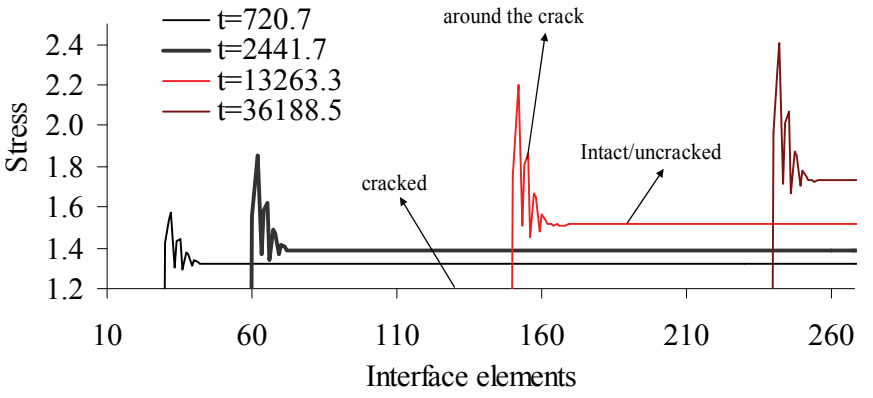

Figure 10: The spatial distribution of stresses along the interface elements at different instant of time (t). The already cracked, around the crack and the intact/uncracked segment are indicated on the stress distribution profiles along the interface

the disparity in time scales among the diffusion and dissolution is portrayed as the accumulation and subsequent recession of the species concentrations, asymptotically reaching nearly-uniform distributions. The progressive dissolution of bonds provides room for the species to diffuse further inside along the interface. Once the bonds are dissolved, diffusion can continue at the site whereas the next bond, if not dissolved, acts as a reflecting barrier to the effective domain of diffusion. The accumulation at the reflecting wall occurs because the time demands for the dissolution of the neighboring bonds are an order of magnitude larger than the diffusion time steps. This accumulation is shown in Figure 6 for intermediate points on the interface. However, with time, further dissolution makes room for the accumulated species and the concentration recesses. Also, the reduction in concentration gradient reduces the accumulation effects.

Dissolution along the interface initiates and propagates the interfacial crack. With the propagating crack, the displacement field changes and the domain of diffusion gets modified. The displacement fields are shown in Figure 7, and the time evolution of displacements of selected nodes are shown in Figure 8. In Figure 8, the time evolution shows that prior to the cracking, displacement gradually increases, and as soon as crack passes the point, the displacement almost remains unchanged. The displacements are exactly opposite in the upper and lower end of the crack (noting that the +ve axis of Y is downward). The mildly noisy nature of the displacement time history (particularly when the crack passes the points) is due to the stochasticity involved in the bond dissolution kinetics. The distribution of stresses along the interface and the time evolution of stresses at selected bonds along the interface are shown in Figure 9 and 10.

Theoretically the stress singularity occurs at the crack tip and the near field stresses are substantially higher and asymptotically decay to the far field stresses. Such distribution of the stresses (σ_{yy}) (in the direction perpendicular to the crack surface) is shown in Figure 10. The fluctuating nature of stress nearing the crack comes because; we plot the stress for all interfacial bonds (elements) rather than the nodes along the interface. Whether some of them are normal to crack surface, others are inclined (45, 135 degree). This is because in the present lattice configuration, a node is connected to its nearest eight neighbors by harmonic springs (which are consistent to D2Q9 lattice configurations (Figure 4) for LBM used for modeling the species migration). Thus the distributions of stress in the normal and inclined elements are different; giving rise of such fluctuations. The time evolution of stresses at particular interfacial element as shown in Figure 9 is consistent with the spatial variations in Figure 10. Peak value of the stresses occurs as the crack passes the interfacial elements and then suddenly drops down to zero to enforce stress free boundary. The noisy variations, once again come from the stochastic time demand

of the bond dissolution, inherent to chemical kinetics.

The rate of dissolution of the interface is strongly influenced by the level of the ambient stress. Following the formulation of the rate law, the stressed bonds have increased chemical potential leading to enhanced rate of the bond dissolution. The rapid dissolution causes the stress corrosion crack to propagate progressively faster, ultimately leading to sudden brittle failure. Thus the time variation of stress gets coupled to the chemistry along the interface. The nature of variation of the rate is shown in Figure 11. Once again, the noisy nature comes from the non-uniform distribution of stresses in the interfacial elements at the propagating front. Aside from the noise, the overall trend of the rate is clean i.e with increasing stress level the rate increases.

With these basic observations on the coupled nature (dissolution chemistry with the mechanical stress) of the interfacial SCC, we simulate the action of the Inhibitors allocated in the system during fabrications. Following the formulation, two kinds of inhibiting mechanism are postulated and illustrated based on the mode of migration of the Inhibiting agents from specific points in the domain to the corroding sites. The driving force for such transport comes from the potential difference between the corroding species and the Inhibitors. The first kind of inhibitor derives the force from the interaction between the corroding species and the inhibitors itself (as common to smart nanoparticles) and the second kind of inhibitors become active in the presence of catalyst a piorio stored in the system, and get released under the action of the enhanced stress around the propagating front (breakage of the microcapsules happens under stresses). Both of this mechanism is dealt with under the framework of LBM.

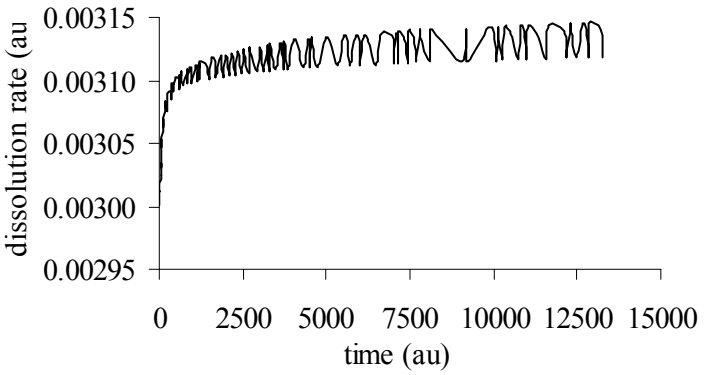

Figure 11: The evolution of stress assisted dissolution rate with time

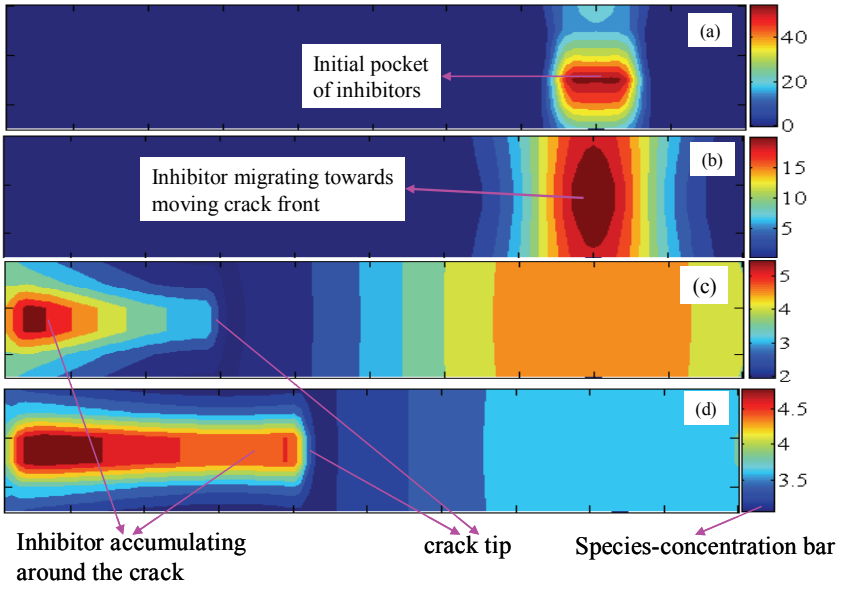

Figure 12: Enrichment of inhibiting agent around the propagating front through migration under long-range inhibitor-species interaction. The densities of agents are shown at time instant of (a) 18 (b) 243 (c) 4347 and (d) 9052 *au* respectively. Accompaning color bar at the RHS shows the field variations of the inhibitor-concentration with varying color

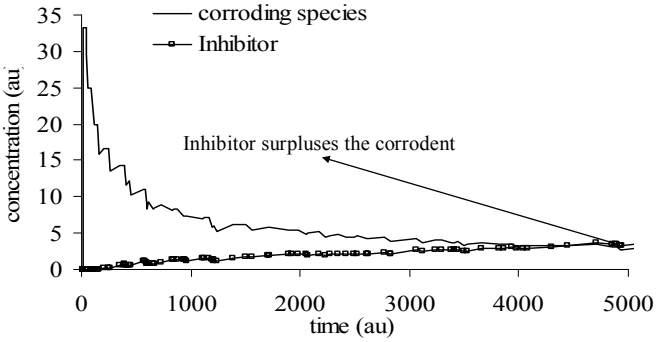

Figure 13: The evolution of species concentration (S) and inhibitor concentration (I) around the propagating crack front. With time, species concentration decreases, whereas the concentration of the Inhibiter increases at the propagating crack front. The increase of Inhibiter is due to the migration towards the crack front and decrease in the corroding species concentration are due to the reduction of concentration gradient along the moving crack front. At some point of time Inhibitor concentration surpluses the corroding one, indicated in the plot

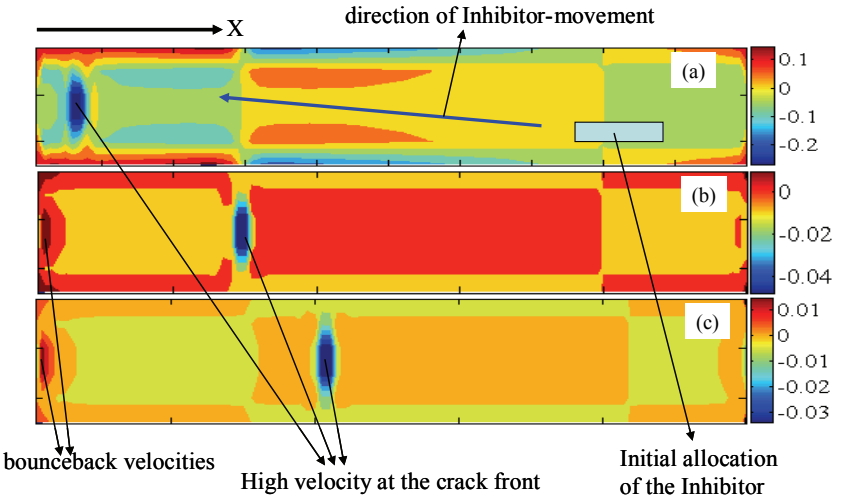

Figure 14: The X-component (along the propagating front) of the velocity field of the inhibitor-migration under the species-inhibitor interactions. Initial allocations of the Inhibitor are indicated in the domain. High velocities (-ve) are located around the moving crack front. The velocities around the boundaries are from the bounce-back conditions enforced at the boundaries. The snaps are at (a) 243 (b) 4347 and (c) 9052 *au* respectively y

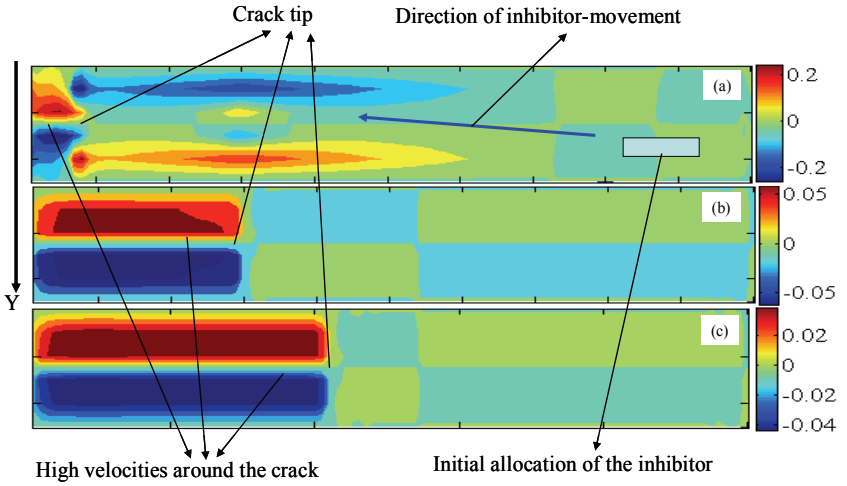

Figure 15: The Y-component of the velocity field (downward normal to the propagating front) under inhibitor-migration interactions. The moving crack front and the initial allocation of the inhibitor are indicated. High velocities are localized around the whole crack. The patches around the boundaries are from the bounce-back condition enforced at the boundaries. The snaps are at (a) 243 (b) 4347 and (c) 9052 *au* respectively

(A) Inhibitors interacting with the corroding species

This is typical to the case of smart nanoparticles [Lee, Buxton and Balazs (2004)] which are driven to the corrosion site under the action of potential difference between the species and the inhibiting agents. Reservoirs of nanoparticles is stored in the system during the fabrication, which are released under demand if required. The inhibitor thus smartly senses the presence of corrosion in the system, moves to the corroding sites to take part in the counteracting kinetics of dissolution-inhibition. The migration takes time and therefore the inhibition becomes effective only after certain time lag as shown in Figure 12. Enrichment of the inhibitor-concentration around the crack is shown from Figure 12. An estimate of the time lag between the triggering and migration can also be obtained from here. Slightly better estimate of the lag and the enhancement of the inhibitor can be better visualized from the time evolution of the species, shown in Figure 13. With the propagating front, the species concentration from the diffusion decays whether the inhibiting agent increases (of course, after the lag of migration). Diffusing species and migrating Inhibitor takes part in the competing kinetics of corrosion and anti-corrosion (healing) respectively. At an instant, the resulting kinetics becomes too slow and thus effectively get arrested. The fluctuations in the evolution of the concentration of the diffusion species comes from the disparity of time scales of diffusion and the bond dissolution resulting in the accumulation and recession of concentration at the propagating front. The respective velocity fields responsible for the transport of the species are shown in Figure 14 and Figure 15, These plots show that the locally enhanced velocity components are responsible for accumulating the inhibitors around the propagating front. The high velocities become prominent (patches) around the crack surface at the later stage, if not earlier. This is in unison to the driving force exerted on the inhibiting particles by the corroding species.

With the migration of the Inhibitors and diffusion of species at the crack tip the kinetics of dissolution and counteractive dissolution start competing each other. The condition of Inhibition is illustrated in the modeling framework presented earlier. High time demand of resultant kinetics implies the condition of effective inhibition, shown in Figure 16. Here, the inhibitions are quantified in terms of effective time demand of the competing mechanism and are expressed in terms of the effectiveness of the inhibiting agent expressed as the activity coefficient(A_i). It is seen that higher activity coefficient leads faster arrest provided other parameters remain identical. The fluctuations in the cumulative time demand curve is due to the stochastic nature of the kinetics. Figure 12 also gives a qualitative estimate of the time required for the effective inhibition to occur which is tailored to the extent SCC already been propagated.

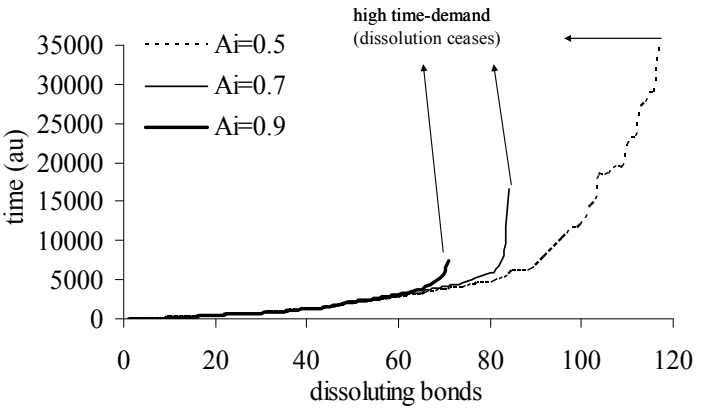

Figure 16: The time demand of the competing kinetics of bond dissolution and inhibition. Time demand means the time taken by an event to occur. Events imply the dissolution of bonds and/or the inhibition of dissolution of a bond. Higher time demands, marked by steep portion of the curves mark the ceasing of the dissolution. Ai is the activity coefficient coefficients of the Inhibitor

(B) Inhibitors interacting with the catalytic particles released around the stressed crack front, from breakage of microcapsules.

The evolution of the system under this kind of Inhibition strategy is illustrated. With such driving force for the inhibitor transport, the evolution of the inhibiting agents is shown in Figure 17. Unlike the action of the Inhibitors in the previous case, these inhibitors gets accumulated only around the propagating front (because of the enhanced stress field prevails only in this region to trigger the release of catalyst). This mechanism is thus more efficient than the previous one where the inhibitors get accumulated around the diffusing species/all around the crack. The time lag inherent to the inhibitor-migration is obvious from the plots. Contrary to the previous case, the enriched regions around the crack tip migrate with the moving crack front. This creeping behavior of the inhibitor is more pronounced in the time evolution of the inhibitor-concentration, shown in Figure 18. While the evolution of the diffusing species remains unchanged, the evolution of the inhibitors is different from that of Figure 13. It is seen that the enriched concentration of inhibitors (represented by cusp) moves as the time evolves. This implies that the inhibitor-enriched region (cusp of concentration) moves with the propagating front under the action of chemical potential around the tip of the crack. This 'creeping' behavior of the inhibitor-enriched zone causes this mode of operation more effective than the previous one shown in Figure 13.

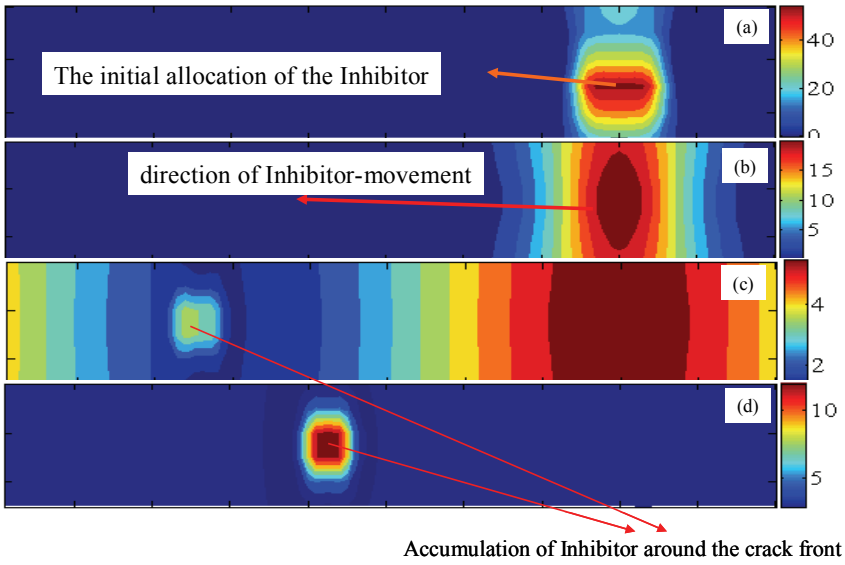

Figure 17: Enrichment of inhibiting agent around the propagating front through migration under long-range inhibitor-catalyst interaction. Release of catalyst is assumed to occur under the enhanced stress field around the propagating crack front. Initial allocation of the Inhibiter in the domain is indicated. The density of the agents are shown at time instant of(a) 18 (b) 243 (c) 3141 and (d) 9052 *au* respectively

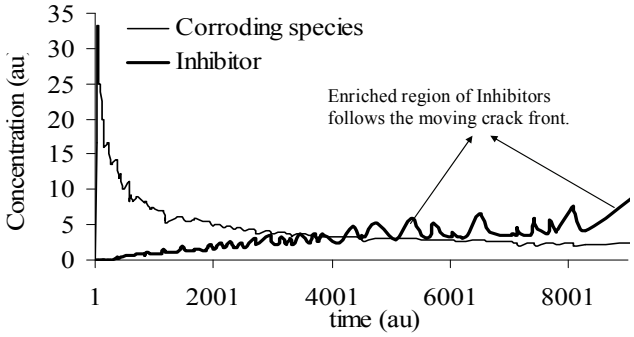

Figure 18: The evolution of corroding species/inhibitor concentrations around the propagating crack front. Inhibitor moves to the crack front after the time of migration. Enriched region of the Inhibitor around the crack front also moves with the moving crack front shown by the cusps in the evolution ofthe inhibitor concentration

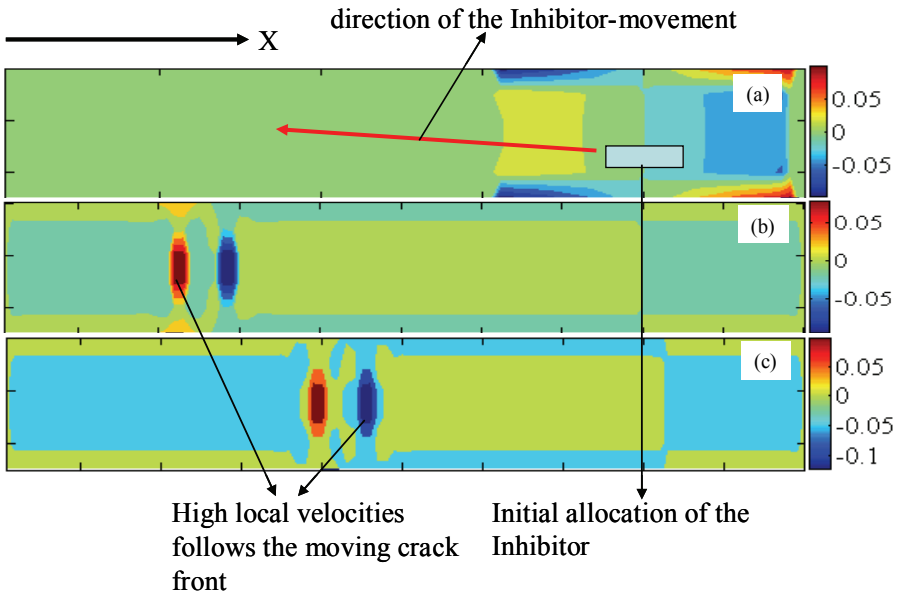

Figure 19: The X-component (along the propagating frcnt) of the velocity field of the inhibitor-migration, under the species-inhibitor Interactions. The velocities around the boundaries are from the bounceback conditions enforced at the boundaries. The snaps are at (a) 243 (b) 3141 and (c) 9052 *au* respectively. Higher velocities are localized right at the crack front The crack front and the initial allocation of the inhibitor are indicated. Unlike Figure 14, there is an additional patch (red) of velocity behind the crack tip. This is due to the fact that the ennched region, which is only around the crack tip (unlike Figure 12) tries to follow the moving crack front. This 'creeping' behavior results this red patch

The velocity fields responsible for the migration are shown in Figure 19 and 20. These fields follow the trend of the potential difference among the nanoparticles and the broken catalytic microcapsules. From the Figure 19 and 20, it is seen that initially the velocity components have higher magnitude around the points of the Inhibitor-allocations, with local patches from the bounceback boundary. Later (close to the Inhibition), two distinct patches of high velocity appears around the propagating crack front. This agrees the fact that the Inhibitors are creeping with the propagating front until the dissolution kinetics get arrested. Both the component of velocities (u_x, u_y) follows this tendencies to assist the enrichment around the crack. Unlike the previous case, the velocity fields are localized only around the propagating front rather than around the whole crack.

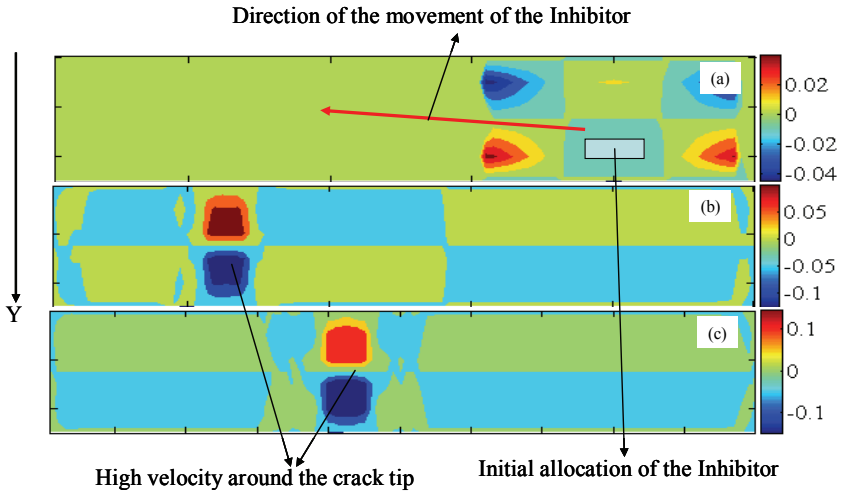

Figure 20: The Y-component of the velocity field (downward normal to the propagating front) under inhibitor-migration interactions. The patches around the boundaries are from the bounceback condition enforced at the boundaries. The snaps are at (a) 243 (5) and (b) 3141(23) au (c) 9052 (40) respectively. The initial allocation of the inhibitor is indicated. Direction of migration is also shown. Two patches of velocities are localized around the crack tip. Unlike Figure 15 (where the high velocities are throughout the crack), the higher velocities are localized at the crack tip only. This makes this mode of operation more effective

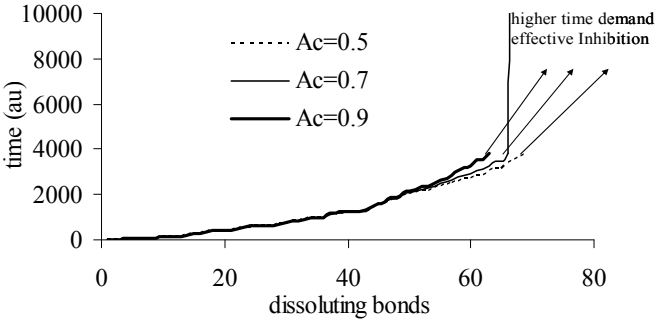

Figure 21: The time demand of the competing kinetics of bond dissolution and inhibition. The time demand means the time taken by an event to occur. Higher time demands, marked by steep portion of the curves represent the ceasing of the dissolution. Ai is the activity coefficient coefficients of the inhibitor

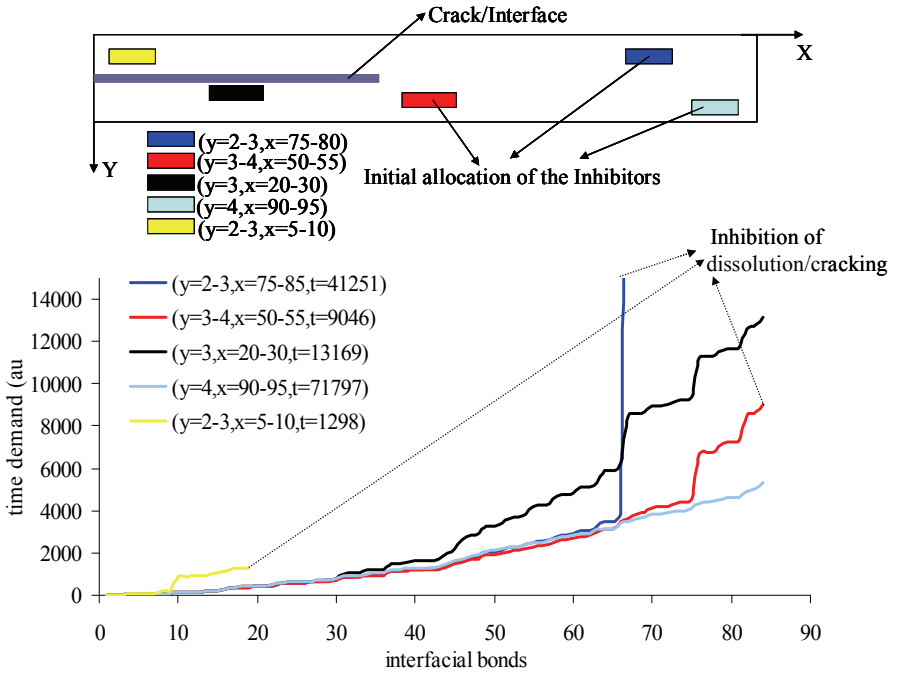

Figure 22: The inhibition efficiency (in terms of time-demand of the competing kinetics of corroding Species and the Inhibitor). The curves correspond to several random locations of the Inhibitors placed inside the domain. Randomly allocated pockets are shown in the domain schematically

Comparing Figure 21 and Figure 16, it is seen that with all the parameters remain unchanged the efficiency of inhibition in the second kind of mechanism is much higher in terms of the effective time of inhibition or arrest of the corrosion kinetics/ propagation of the crack front. The inhibition consequently is less sensitive to the activity of the inhibitors than the previous case, indicated in the almost identical trend of the time demand of the resultant kinetics.

We check the robustness of the inhibition w.r.t the random locations of the inhibitors initially placed in the domain. With all others conditions (i.e concentration of inhibitors at random locations, the activity coefficients etc) remain identical; the inhibition efficiency is depicted in Figure 22, for the positions of the inhibitors allocated randomly inside the domain. Out of five cases considered, though the time demands changes quite a few order of magnitude but for out of five three cases, the extent of propagation of crack before it get arrested by the inhibition remains unchanged.

This is not the case for case 6 though, where inhibition took place much earlier, because of concentration of the inhibitors near the initiation of the crack front. Thus it is seen that the inhibition efficiency is statistically similar with respect to the random allocations of the inhibitors inside the domain, whereas the exceptional few cases (extreme or rare events) the effective time of inhibition could vary radically (either too earlier or too late) owing to the allocations at several locations right aside the interface (crack) or away from the interface.

4 Conclusions

We presented a coupled framework of computations by combining several models/methods spanning over several scales governing the physical regime typical to the phenomena of interfacial stress corrosion and cracking. The SCC is presented by coupling the diffusion of the species, dissolution of interfacial bonds accompanied by the propagation of crack front. The chemistry acts in conjugation with the mechanics to explore the coupled multiphysics nature of the system. The inhibition mechanisms are stated and modeled to capture their efficacy in preventing the kinetics of bond dissolution and subsequent arrest of the crack. The sensing of the corrosion are shown to be achieved through the interactive force among the inhibiting agent and the ingressing chemical/ and or catalyst a priori allocated in the system. The driving force results from the chemical potential difference between them. Two alternative mechanism of triggering the inhibition is proposed. Empirically defined potential are used to model the potential of corroding species and the inhibitors. The migration of the inhibiting agents is described under the framework of the Boltzmann Transport equation and solved on a lattice representing the domain. The efficiency of the inhibiting mechanism is quantified in terms of the competence of the dissolution and the counteractive kinetics. The robustness of the proposed mechanism is also been qualitatively inferred in the context of the random allocations of the inhibitors in the domain.

Acknowledgement: This research was supported by the U.S Army Research Office, under the cognizance of Dr. Larry Russel. This research was also supported by the World Class University (WCU) program through the National Research Foundation of Korea funded by the Ministry of Education, Science and Technology (Grant no.: R33-10049). The second author is also pleased to acknowledge the support of the Lloyd's Register Educational Trust (LRET) which is an independent charity working to achieve advances in transportation, science, engineering and technology education, training and research worldwide for the benefit of all.

References

Alava M. J., Nukala P., Zapperi S. (2006) Statistical models for fracture. *Adv Phys* 55: 349–476.

Brown E. N., White S. R., Sottos N. R. (2005) Retardation and Repair of fatigue cracks in a microcapsule toughened epoxy composite – Part I: Manual infiltration. *Composites Science and Technology*, 65, 2466-2473.

Dry C. (1994) Matrix cracking repair and filling using active and passive modes for smart timed release of chemicals from fibres into cement matrices. *Smart Materials and Structures* 3(2) 118-123.

Fitzgerald G., Goldbeck-Wood G., Kung P., Petersen M., Subramanian L., Wescott J. (2008) Material Modeling from Quantum Mechanics to Mesoscale. *CMES: Computer Modeling in Engineering and Sciences*, 24, 3, 169-183.

Fontana, M. G. (1986) Corrosion Engineering, *McGraw Hill*, New-York.

Gutpa S., Zhang Q., Emrick T., Balazs A. C., Russell T. P. (2006) Entropy-driven segregation of nanoparticles to cracks in multilayered composite polymer structures. *Nature Materials* (5) 229-233.

Ho C. F., Chang C., Lin K. H., Lin C. A. (2009) Consistent Boundary Conditions for 2D and 3D Lattice Boltzmann Simulations. *CMES: Computer Modeling in Engineering and Sciences*, 44, 2, 137-156.

Jakab M. A., Scully J. R. (2005) On demand release of corrosion inhibiting ions from amorphous Al-Co-Ce alloys, *Nature Materials* 4, 667-670.

Kamaya M., Itakura M. (2009) Simulation for intergranular stress corrosion cracking based on a three-dimensional polycrystalline model, *Engineering Fracture Mechanics* 76,386–401.

Lufrano J., Sofronis P. (2000) Micromechanics of Hydride Formation and Cracking in Zirconium Alloys, *CMES: Computer Modeling in Engineering & Sciences*, 1, 2, 119-132.

Lamaka V. S., Shchukin D. G., Andreeva D. V., Zheludkevich M. L., Mohwald M, Ferreira M. G. S. (2008) Sol-Gel/Polyelectrolyte Active Corrosion Protection System, *Advanced Functional Materials*, 18, 3137–3147

Lee J. Y., Buxton G. A., Balazs A. C. (2004) Using nanoparticles to create self-healing composites, *Journal of Chemical Physics* 121 (11) 5531-5540.

Mullin W. M., Shumaker E. J., Tyler G. J. (1997) Stochastic Kinetics of Corrosion and Fractal Surface Evolution, *Journal of Corrosion Science and Engineering*, (1)-7.

Nishidate Y., Nikishkov G. P. (2008) Atomic-scale modeling of self-positioning

nanostructures, *CMES: Computer Modeling in Engineering and Sciences*, 26, 2, 91-106.

Nishimura K., Miyazaki N. (2001) Molecular dynamics simulation of crack propagation in polycrystalline material, *CMES: Computer Modelling in Engineering and Sciences*, 2, 143.

Srivastava D., Atluri S. N. (2002) Computational Nanotechnology: A Current Perspective, *CMES: Computer Modeling in Engineering & Sciences* 3-5,531-538

Shan X., Chen H. (1993) Lattice Boltzmann Model for simulating flows with multiple phases and components. *Physical Review E* 47:1815-1819.

Succi S. (2001) The Lattice Boltzmann Equation for Fluid Dynamics and Beyond, *Clarendon Press*, Oxford.

Trenado C., Strauss, Wittmar M. (2008) Hybrid Multiscale Modeling of Corrosion Nanoinhibitors Transport *Proceedings of the COMSOL Conference*, Hannover.

White S. R., Sottos N. R., Geubelle P. H., Moore J. S., Kessler M. R., Sriram S. R., Brown E. N., Viswanatham S. (2001) Autonomic healing of polymer composites, *Nature* 409 (6822) 794.

Yakobson B. I., Shchukin E. D. (1993) Environmentally enhanced instability of stressed solids. *Journal of Materials Science* 28, 4816-4820.

Zheludkevich M. L., Serra M., Mon-temayor M. F., Yasakau K. A., Miranda Salvado I. A., Ferreira M. G. S. (2005) Nanos-tructured sol-gel coatings doped with cerium nitrate as pre-treatments for AA2024-t3 corrosion protection performance, *Electrochim. Acta* 51, 208-217.